Journal of Applied Fluid Mechanics, Vol. 11, No. 3, pp. 527-544, 2018.
Available online at www.jafmonline.net, ISSN 1735-3572, EISSN 1735-3645.
DOI: 10.29252/jafm.11.03.28028

Investigation of the Numerical Methodology of a Model Wind Turbine Simulation

N. Tabatabaei[1†], M. J. Cervantes [1,2] and C. Trivedi [2]

[1] *Department of Engineering Sciences and Mathematics, Luleå University of Technology, Luleå, SE-97187, Sweden*
[2] *Department of Energy and Process Engineering, Norwegian University of Science and Technology, Trondheim, NO-7491, Norway*

†*Corresponding Author Email: narges.tabatabaei@ltu.se*

(Received May 22, 2017; accepted December 23, 2017)

ABSTRACT

The present work aims to investigate different methodologies for the numerical simulation of an upwind three-bladed wind turbine; which is supposed to be a base model to simulate icing in cold climate windmills. That is a model wind turbine for which wind tunnel tests have been completed at the Norwegian University of Science and Technology (NTNU). Using the assumption of axisymmetry, one-third of rotor has been modeled and periodic boundaries applied to include the effects of other blades. Then the full rotor was studied with transient simulation. To take in the effects of wind turbine wakes, the wind tunnel entrance and exit have been considered 4 and 5 diameters upstream and downstream of the rotor plane, respectively. Furthermore, the effects of tower and nacelle are included in a full-scale transient model of the wind tunnel. Structured hexa mesh has been created and the mesh is refined up to y+=1 in order to resolve the boundary layer. The simulations were performed using standard k-ε, Shear Stress Transport (SST) model and a sophisticated model Scale-Adaptive Simulation (SAS)-SST to investigate the capability of turbulence models at design and off-design conditions The performance parameters, i.e., the loads coefficients and the wake behind the rotor were selected to analyze the flow over the wind turbine. The study was conducted at both design and off-design speeds. The near wake profiles resulted from the transient simulation match well with the experiments at all the speed ranges. For the wake development modelling at high TSR, the present simulation needs to be improved, while at low and moderate TSR the results match with the experiments at far wake too. The agreement between the measurements and CFD is better for the power coefficient than for the thrust coefficient.

Keywords: Model wind turbine; CFD; Transient; Wake profile; Turbine performance.

1 INTRODUCTION

In recent years, wind energy has become one of the most economical renewable energy technologies. As the environmental matters become more important and as the world is striving to find cleaner sources of energy, the portion of electricity that is wind generated is likely to increase substantially every year. Windmills are now introduced in cold areas to meet the global energy demand. Conventionally, wind turbines are designed for climate without icing, and installation in cold climate pause certain challenges for which they are not designed. Icing on the turbine blades often lead to operational instability. This affects dynamic performance due to imbalanced load.

Several studies of icing on the turbine blades have been reported, mainly from the arctic region, since 1990 (Tammelin *et al.* 1998; Frohboese and Andreas 2007; Zhao *et al.* 2009). Nevertheless, no detailed measurements on the dynamic characterization of a wind turbine blade in icing condition are reported. In the absence of test data, investigations largely rely on numerical techniques. Such analysis is performed using simplified Blade Element Momentum (BEM) or Vortex Wake models. The most recent approach is the complete 3D Computational Fluid Dynamics (CFD), which is based on solving the mass and momentum equations. Previous CFD studies of icing condition consist of 2D airfoil (Homola *et al.* 2011; Turkia *et al.*2013) and a rotor without the turbine components (Reid, Baruzzi, Ozcer, Switchenko, & Habashi, 2013).

In the absence of experimental data, trustworthy CFD analysis is vital, which demonstrates the credibility of the numerical results. For such analysis, a multistage approach is followed: (1) an

accurate CFD model of a wind turbine free of ice, (2) an accurate CFD model of airfoils subject to ice and (3) simulation of the complete turbine under icing condition. The present work focuses on the first approach, i.e. investigations of different conditions to perform accurate numerical simulations of a wind turbine. For the validation, available experimental data from the benchmark studies are considered. Three test cases are available in the literature, which are briefly described below with the main corresponding simulations performed. The object is to highlight the research work performed until now in this field in order to motivate the focus of this work.

Two-bladed NREL Phase VI

In 2006, National Renewable Energy Laboratory (NREL) conducted series of measurements on a wind turbine (10 m rotor diameter) in NASA-Ames wind tunnel. The measurements included the computation of power and thrust coefficients at different tip-speed-ratio (TSR), i.e., 2-11. Researchers have worked to simulate the turbine using different methods (Schreck, 2008), (Schepers & van Rooij, 2008). N. Sorensen *et al*. (Sørensen *et al*. 2014) modeled a simplified geometry of the blade, beside the tower and tunnel walls. The numerical model showed difficulty to predict the turbine power and thrust, particularly in separated flow conditions, where the error is large. Later, in 2008, the simulations conducted by R.P.J.O.M. van Rooij and E.A. (Rooij and Arens 2008; Schreck 2008) showed good agreement with the experimental data at low wind speeds. An isolated rotor was modeled considering the periodical boundaries. Numerical studies with different turbulence models, k-ω SST and Detached Eddy Simulation (DES), were conducted and the difference was negligible. In 2009, S. Gomez-Iradi *et al*. (Gomez-Iradi and Barakos 2008; Gomez-Iradi *et al*. 2009) performed the unsteady simulations using k-ω and k-ω SST as the turbulence models. In the case of separation at high inlet velocity, the turbulence models showed large error. Numerical error in the torque value was 18% at the design point. They concluded that the tower must be taken into account to capture the integrated loads of the blade, i.e. thrust and power.

Mexico Rotor: Three-bladed NREL Phase VI

Later in 2006, wind tunnel tests were conducted on a three-bladed wind turbine. The studies were focused on the investigations of velocities and wake behind the rotor. Many research centers have worked to analyze this model using different numerical methods (summarized in Schepers*et al*. 2012). Different approaches of numerical modelling were applied starting from complete wind tunnel to an isolated rotor.

In 2011 (Bechmann *et al*. 2011), the near wake (one diameter downstream) measurements were reproduced by CFD. They observed differences which were addressed to the laminar flow at the leading edge of the tested wings, while the simulations were run fully turbulent. They also suggested taking into account the tunnel effect which was skipped in that simulation. Furthermore, the influence of tower was found to be noticeable in the near wake (Lutz 2011). The wake computations in 2014 (Sørensen *et al.* 2014) showed that within one rotor diameter downstream of the rotor, excellent agreement can be obtained for all three velocity components as illustrated by the axial transects. They also indicated that the nacelle needs to be included in wake studies of the MEXICO turbine. In 2015 (Carrión *et al*. 2015), the wake profile validation extended up to one and a half rotor diameters downstream. Overall, fair agreement was obtained with the computational fluid dynamics showing good vortex conservation near the blade. The calculation of the pressure distributions and the integrated thrust and torque were at the same level of the previous studies have encountered discrepancies with the experiments, especially in low wind velocities (Schepers *et al*. 2012). The loads along the blade were consistently over-predicted by the numerical model.

Three-bladed NREL with S826 profile section

In 2011, the performance characteristics and the near wake of a model wind turbine were investigated in a low-speed, closed-return wind tunnel at the Norwegian University of Science and Technology (NTNU), Norway (Krogstad and Adaramola 2012; Krogstad and Eriksen 2013) named as NTNU test case in the following. The tested model was a three-bladed wind turbine with a rotor diameter of 0.90 m. Power and thrust coefficients at different TSR values (2-11) were measured.

In 2011 (Krogstad *et al.* 2010; Krogstad and Lund 2012), numerical calculations were performed by means of fully 3D CFD simulations. The predicted power coefficients were close to the measurements, however, at high TSR the power coefficient was overestimated by the numerical model. At the design TSR, the power coefficient was around $\pm 2\%$ of the experimental value. In 2014, E. Manger *et al*. (Kalvig & Manger 2011; Kalvig *et al*. 2014) focused on the calculation of wake velocity as well as the power and thrust coefficients. The time-averaged results were close to the measurements on the design point (error <7%) but, at both high and low TSR values, the error was up to 92%. The axial velocity profiles across the wake were calculated in both near wake and far wake (5D). For the near wake, the results were close to the experiments. Short calculation time caused insufficient averaging that imposed more deviations in farther wake profiles. Considering the interaction between the turbine tower and the rotor blades, the asymmetry in the wake profiles were captured as it was observed in the experiments. Hansen (Hansen 2010) improved the accuracy of the isolated rotor simulation, by using a transition model. The predictions of Hansen for power and thrust were in close agreement over the full range of TSR, even in the fully stalled region (Krogstad and Eriksen 2013). At farther wakes, the results were not accurate, not near the center nor the whole wake width. In 2014, Luca Oggiano (Oggiano 2014) modeled the isolated rotor with a part of the nacelle

in a large far field. Results relative to rotor loads, power production and thrust force show good agreement with the experiments and the results from the near wake computations were in partial agreement with the experiments. The local differences were addressed to the simplified geometrical model used in the simulation.

Considering the turbine characteristics reproduced by the previous numerical studies, results agreed well with the experiments at the design point. However, at off-design the power and thrust estimations have been challenging at both stall condition and high rotational speeds. The simulation configuration has been influencing the results, as well as the modeled downstream length. The interaction of the isolated rotor with the tower, nacelle, and tunnel walls is needed to investigate thoroughly their effects. Insufficient grid resolution played a critical role in resolving the flow features at off-design conditions. The quality of the grid cells should be considered along with the least simplifications in the geometry. Enough simulation time is required for a reliable time averaged results in the transient simulations as suggested in the literature.

Since the performance characteristics consist of integrated values, it is necessary to analyze more in details the flow for a reliable validation. Although the numerical data at the near wake are generally close the experimental results, the development of the wake is not modeled properly especially at high rotational speeds. Far wake profiles have rarely been modeled and discussed, which requires modeling nearly the whole system experimentally considered.

The wake development should be investigated, because in the wind farms it can determine the upstream condition of the following turbine row. Such effect is expected to be more pronounced in icing conditions. Furthermore, it results in a higher level of CFD validation as it reveals the diffusion capability of the numerical tool. In this paper, the numerical simulation of the NTNU upwind three-bladed wind turbine model (Krogstad and Eriksen 2013) is presented and analyzed in detail.

2 TEST CASE

The experiments were performed in a large low-speed closed return wind tunnel. The tunnel has a test-section of 1.9 m (height) × 2.7 m (width) × 12.0 m (length). All tests reported here were performed in a uniform inlet flow at a turbulence level of about 0.3%. The wind turbine tested has a 3-bladed upwind rotor and the overall rotor diameter is 0.9 m.

The rotor blade geometry was designed using a blade element momentum method developed in-house. The S826 NREL wind turbine airfoil section is used throughout the span of the blade. The main purpose of the referenced experiments was to provide data for the verification, rather than to simulate the performance of a specific full-scale turbine. Therefore, the blade chord length was made about 3 times wider than what is typical on commercial turbines to reduce the gap in Reynolds number. The torque generated by the wind turbine was measured by a torque sensor mounted directly on the nacelle. The forces on the model were obtained from a six-component force balance on which the model was mounted. The rotor angular speed was varied from Ω= 10.5 to 249 rad/s, which gave a TSR ($\Omega R/U_\infty$) of 0.5 to about 12 based on the freestream velocity U_∞ (meter per second) used for the measurements. R is the radius of the rotor in meter (Krogstad *et al*. 2010). For the wake measurements, a Pitot-static pressure probe was used to measure the time-averaged streamwise velocity field in the upper half of the wake at different downstream locations from the turbine. The wake velocity field in the cross-stream plane was measured over a 5 mm uniformly space grid (Krogstad and Lund 2012).

The measured values presented in (Krogstad and Lund 2012) are used as a dataset for the load performance on the blades, as well as the wake profiles. For a turbine operating under constant wind speed, the power output from a wind turbine can be expressed by the power coefficient, $C_p = 2T\Omega/R^2U_\infty^3$, where T is the torque generated by the rotor, ρ is the air density). The load on the turbine is represented by the thrust coefficient and defined as $C_T = 2D/R^2U_\infty^3$, where D is the drag force (Krogstad and Adaramola 2012).

The blade pitch is assumed to be a considerable source of uncertainty as mentioned in (Adaramola and Krogstad 2011). Furthermore, the drag force acting on the tower and nacelle system was measured without the rotor blades at the same freestream velocity used for the performance measurements in order to compensate for the tower and nacelle thrust. The effective thrust acting on the

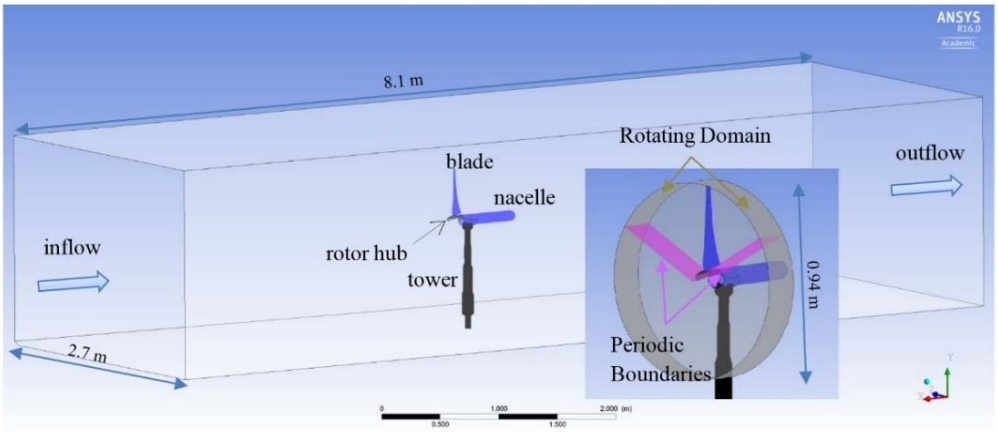

Fig. 1. The model sketch and the boundaries.

rotor system during the operation was then estimated by subtracting the tower and nacelle system drag from the thrust acting on the whole system (Karlsen 2009; Krogstad and Adaramola 2012).

The experimental performance characteristics of the model turbine were repeated several times during the study. The maximum deviation in the maximum C_P is reported to be less than 2% (Krogstad and Adaramola 2012).

3 NUMERICAL MODEL

A CFD solver ANSYS CFX 16.0 was used to conduct the numerical studies. The incompressible unsteady Reynolds-averaged Navier-Stokes (URANS) equations were solved on a multi-block structured grid. High-resolution scheme for spatial discretization and the second-order backward difference for time derivative were used throughout the simulation. The convergence criteria was set to a root-mean-squared value less than 10-6. In steady state simulation, different interface models between

the stationary (i.e., wind-tunnel and the wind turbine tower and nacelle) and rotating parts exist, because 'rotation' basically is a time depending process. Indeed, the physical position of each point in the rotating part is changing toward the stationary part during the rotation.

The 'Stage' model, used in this work, circumferentially averages the fluxes in bands and transmits the average fluxes to the downstream component, mimicking the mean flow. So, such method seems to be more appropriate to get average engineering quantities such as thrust and power coefficients compared to the 'Frozen Rotor' models which maintain a fixed initial relative position of the components. It will be discussed more in "Geometry" section.

3.1 Geometry

The geometrical model comports the complete wind turbine with tower and nacelle (Fig. 1). Wind tunnel inlet and outlet boundaries are 4 and 5 diameters upstream and downstream of the rotor plane, respectively. This will allow investigating the wake behind the rotor. The wake profiles are studied downstream of the rotor at axial distances (X) from the rotor. One diameter downstream the rotor (X/D=1) is considered as the near wake while four diameters downstream (X/D=4) shows the developed wake.

3.2 Turbulence Modeling

The k-ω SST turbulence model is a two-equation eddy-viscosity model which has become very popular. The use of a k-ω formulation in the inner parts of the boundary layer makes the model directly usable all the way down to the wall through the viscous sub-layer, hence the SST k-ω model can be used as a low-Re turbulence model without any extra damping functions. The SST formulation also switches to a k-ε behavior in the free-stream and thereby avoids the common k-ω problem that the model is too sensitive to the inlet free-stream turbulence properties (CFD online.2011).

The k-ω based Shear-Stress-Transport (SST) model was designed to give a highly accurate prediction of the onset and the amount of flow separation under adverse pressure gradients by the inclusion of transport effects into the formulation of the eddy-viscosity [36]. Since wind turbines geometries are potential to cause flow separation, shear stress transport model with automatic wall function was activated to model the flow. Reynolds stress models are performing well to model rotating fluids (*ANSYS CFX-solver modeling Guide Release 15.0.* 2013). Such models were tested. Unfortunately, a good convergence could not be reached in the present case. The k-ω SST model was finally chosen to model turbulence in this work.

In the case of transient simulations, Scale-Adaptive Simulation (SAS) SST model was used to resolve the wake behind the turbine. While today's CFD simulations are mainly based on Reynolds-Averaged Navier-Stokes (RANS) turbulence models, it is becoming increasingly clear that certain classes of flows are better covered by models in which all or a part of the turbulence

spectrum is resolved in at least a portion of the numerical domain. Such methods are termed Scale-Resolving Simulation (SRS) models (Menter 2012). This model performs like standard RANS models in steady flows, but enable the formation of a broadband turbulence spectrum for certain types of unstable flows. The difference between standard RANS and SAS models lies in the treatment of the scale-defining equation; typically, dissipation (ε, ω), or turbulent length scale equation. In classic RANS models, the scale equation is modeled based on an analogy with the k-equation using dimensional arguments. The scale equation of the SAS model is based on an exact transport equation for the turbulence length scale (*ANSYS CFX-solver modeling Guide Release 15.0* .2013).

Choosing a turbulence model imposes a specific wall treatment. In addition to the different formulations of k-ε and k-ω SST models in the inner parts of the boundary layer, the flow near the wall is modelled differently. The "scalable wall-functions" used in the k-ε model are based on physical assumptions that are problematic, especially in the flows at lower Reynolds numbers (Re<105), as the viscous sublayer portion (y^+<11) of the boundary layer is neglected in the mass and momentum balance (*ANSYS CFX-solver theory Guide Release 15.0.*2013). It is, therefore, desirable to use a formulation which will automatically switch from wall-functions to a low-Re near wall formulation as the mesh is refined. The k-ω model of Wilcox contains an analytical expression for ω in the viscous sublayer. The main idea behind the formulation proposed in ANSYS CFX is to blend the wall value for ω between the logarithmic and the near wall formulation. The "automatic wall treatment" allows a consistent y+ insensitive mesh refinement from coarse grids, which do not resolve the viscous sublayer, to fine grids placing mesh points inside the viscous sublayer (*ANSYS CFX-solver theory Guide Release 15.0.*2013). There is a blending function and it is weighting between the two regions allowing a smooth increase towards the wall function as y+ is increasing. It means that even in the case of y^+=6, the solution is approaching to the "low Reynolds number" method while still using some empirical formulas for the ω value in the viscous sublayer.

In order to evaluate the performance of wall functions in the case of wind turbines, we have used three types of mesh with different y^+ values on the blade wall. Regarding y^+ definition, it is a function of wall shear stress in addition to the first node position on the wall. Therefore, it would vary in different TSR with the same mesh size, as well as throughout the blade wall. The average value through the blade surfaces is considered, while the distance of the first node from the wall is kept fixed at different TSR.

3.3 Boundary Condition

There is a uniform inflow at a wind speed of U_∞=10.0 m/s. The turbulence intensity is set to be 0.3% at the inlet based on the referenced experiments. "No slip" condition is used for the walls, i.e., the fluid immediately next to the wall assumes the velocity of the wall, which is zero. The outlet boundary condition is set to an "opening" which allows the fluid to cross the boundary surface in either direction, with zero relative pressure. The rotor speed for the design TSR of 5.79 is 1230 rpm. It results in a rotor tip Reynolds number $Re=U_\infty(2R)/\upsilon$ of 103 600, where ν is the air kinematic viscosity. The rotational speed is varied to investigate the other TSR values: 3.335 and 9.15. In order to reduce the computational costs in steady state simulations, periodic boundaries are applied in the rotating part. It's assumed that the flow in 1/3 of the rotor is identical to the two other thirds.

3.4 Grid

A multi-block structured grid contains an unstructured arrangement of hexahedral blocks, where each block contains a structured grid.

The mesh contains the hub, nacelle and the tower inside the wind tunnel. Mesh was created using ICEM CFD software. The multi-block topologies employed for this work start from a C-topology around the blade in order to resolve the suction peak on each blade section as well as the trailing edge vortex shedding (Fig. 2).

Such topology prevents low-quality hexahedral cells around the extremely sharp trailing edge geometry of the blade tip. The mesh allows for variations of the pitch angles along the blade height without reducing the quality near the blades. A hexahedral multi-block mesh was also generated in the wind tunnel for the stationary domain. Starting at the tunnel inlet, the mesh contains the tower and horizontal nacelle and end at the tunnel outlet. This hexahedral mesh is made of one multi-block connected to the cylinder shell of the rotating domain with the general grid interface (GGI).

Different configurations of the boundary layer are investigated, i.e., wall function or complete resolution of the boundary layer up to y^+<1. Refining the first cell on the blade wall leads to a considerable increase number of cells in the whole domain, when the same quality is expected. In the other words, the near wall cells were set first, and then extended throughout the whole domain with an appropriate size ratio that ensures a good quality. The main approach to generate the meshes relies on satisfying the quality criteria. In each mesh, once the quality is satisfied, the number of nodes was assumed to be sufficient.

Furthermore, the mesh convergence test is performed to make sure that the mesh is dense enough with each certain size of the first cell (Fig. 3). For the case shown, 1.5 M nodes are required and a denser mesh results in a similar value (error<1.2%) for the load coefficients.

The mesh used in this study consists of two separate grids for the rotating and stationary domains connected by a general grid interface. Table 1presents three configurations of meshes generated

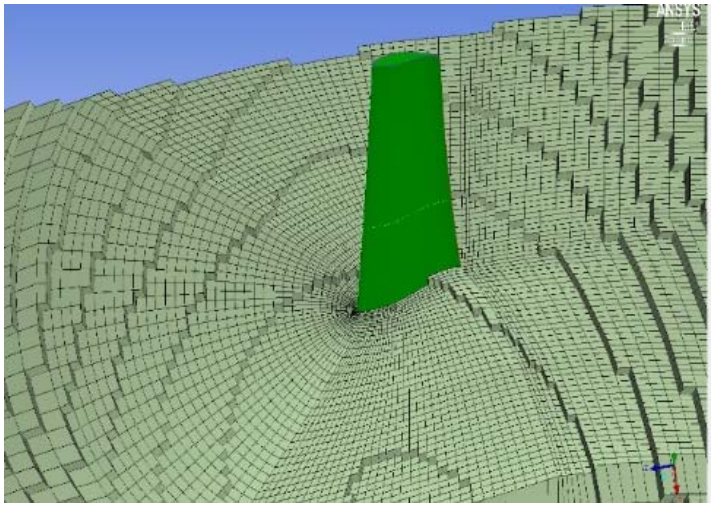

Fig. 2. Mesh configuration on a radial section of the blade at the rotating domain.

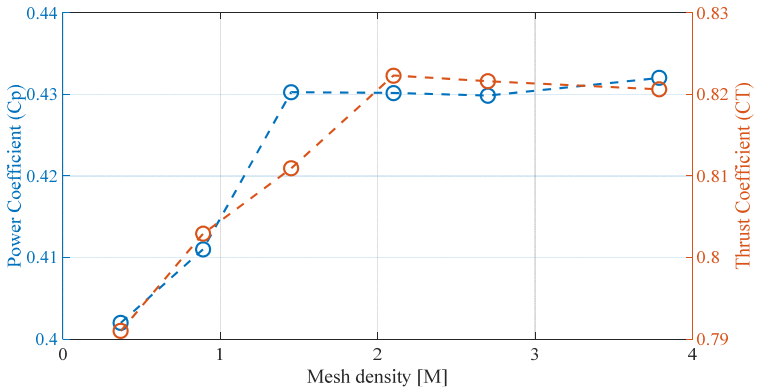

Fig. 3. Mesh sensitivity analysis for case II of table 1 in the steady state simulation.

for the rotating and stationary domains. As the most important criteria for a standard mesh (*ANSYS CFX-solver manager user's guid.*2009), 'angle', 'volume change' and 'quality' of the cells were checked to meet the limitations in each case. The quality is based on the definition in ANSYS ICEM CFD. To analyze the effect of wall treatments, three cases are studied based on the y^+ value on the blade and the mesh density. As mentioned, based on the y^+ value, the whole mesh density is tuned to maintain a consistent coarseness and quality throughout the mesh. The resultant mesh densities in the both domains are reported in Table 1, in addition to the quality conditions.

4 Results And Discussion

The goal of this work is to study the simulation methods and compare them to the available measurements for evaluation. So, the integrated parameters, i.e., the load coefficients are evaluated as well as the detailed velocity profiles in the wake downstream. Load coefficient values are the integral of the load distribution through the blade surfaces from the hub section to the tip, thus it may not be a comprehensive representation of the flow performance. In the next step, velocity profiles are studied at the wake behind the turbine to analyze the simulations more in details.

The performed simulations and the corresponding numerical specifications are listed in Table 2. The main simulations include cases 1 to 18. Simulations 19 to 25 are concerned with a sensitivity analysis of different modeling parameters. The inlet velocity for all cases has been 10 m/s.

4.1 Modeling Effect

Domain periodicity

In order to see how important, the differences are on the boundary planes between the blades (shown in Fig. 1), some simulations have been performed modeling the whole rotor to be compared with the model of one-third of rotor assuming periodicity. Both the steady state and transient simulations are considered.

Regarding Table 2, cases 20 and 5 are compared, through which the effect of periodicity assumption in steady state simulations can be analyzed. The results show 2.7 % difference in the rotor thrust coefficient, 10% difference in the thrust of the whole machine (including the tower, nacelle, …),

Table 1 Detailed mesh specifications in the employed CFD grids

	Rotating Domain					Stationary Domain	y+ average in design speed
Case	number of nodes (1/3 of rotor) [M]		% poor	% acceptable	% good	number of nodes (1/3 of rotor) [M]	
I	0.6	aspect ratio	0	<1	100	1.5	58.3
		orthogonal angle	<1	6	94		
		expansion factor	<1	1	99		
II	1.5	aspect ratio	0	1	99	1.5	6.4
		orthogonal angle	<1	15	85		
		expansion factor	<1	<1	100		
III	15	aspect ratio	1	2	97	6.7	0.3
		orthogonal angle	<1	16	84		
		expansion factor	<1	<1	100		

Table 2 specifications of the simulated cases

Simulation #	Ω (rpm)	TSR	Turbulence model	y+	Simulation type	configuration
1	74.44	3.35	k-ω SST	0.22	Steady/Stage	Periodic 1/3 rotor
2	128.67	5.79	k-ω SST	0.3	Steady/Stage	Periodic 1/3 rotor
3	203.33	9.15	k-ω SST	0.44	Steady/Stage	Periodic 1/3 rotor
4	74.44	3.35	k-ω SST	5	Steady/Stage	Periodic 1/3 rotor
5	128.67	5.79	k-ω SST	6.4	Steady/Stage	Periodic 1/3 rotor
6	203.33	9.15	k-ω SST	9.6	Steady/Stage	Periodic 1/3 rotor
7	74.44	3.35	k-ω SST	39	Steady/Stage	Periodic 1/3 rotor
8	128.67	5.79	k-ω SST	58.3	Steady/Stage	Periodic 1/3 rotor
9	203.33	9.15	k-ω SST	78.6	Steady/Stage	Periodic 1/3 rotor
10	74.44	3.35	k-ω SST	0.22	transient	full rotor
11	128.67	5.79	k-ω SST	0.3	transient	full rotor
12	203.33	9.15	k-ω SST	0.44	transient	full rotor
13	74.44	3.35	k-ω SST	5	transient	full rotor
14	128.67	5.79	k-ω SST	6.4	transient	full rotor
15	203.33	9.15	k-ω SST	9.6	transient	full rotor
16	74.44	3.35	k-ω SST	39	transient	full rotor
17	128.67	5.79	k-ω SST	58.3	transient	full rotor
18	203.33	9.15	k-ω SST	78.6	transient	full rotor
19	128.67	5.79	k-ω SST	0.33	Steady/Stage	full rotor
20	128.67	5.79	k-ω SST	6.4	Steady/Stage	full rotor
21	128.67	5.79	k-ε	58.3	Steady/Stage	Periodic 1/3 rotor
22	128.67	5.79	k-ε	6.4	Steady/Stage	Periodic 1/3 rotor
23	128.67	5.79	k-ω SST	58.3	Steady/frozen rotor	Periodic 1/3 rotor
24	203.33	9.15	k-ω SST	0.44	Steady/frozen rotor	Periodic 1/3 rotor
25	128.67	5.79	SAS SST	58.3	transient	full rotor

and 3 % difference in the power coefficient. In the above simulations boundary layer was resolved partly since the average y^+ on the blade was '6.4'.

Similar simulations were performed comparing cases 2 and 19 (Table 2), in which the boundary layer was fully resolved (mesh: Table 1, case III). The difference in load coefficients is less than 1%.

From these two comparisons, it can be concluded that the periodicity is a proper assumption if the mesh is refined enough and the boundary layer is fully resolved. In this case, the load coefficients of the rotor are almost unchanged (error<3%) due to the periodicity assumption. Otherwise, the accuracy decreases, especially in the thrust evaluation of the whole machine.

The tower is the main element disturbing the periodicity of the real flow in the blade sectors. In the steady state simulations, any time variation was averaged with the 'stage' interface (it will be discussed later in 0). So, none of the periodic surfaces are affected directly by the presence of the tower

Wake velocity profiles in Fig. 4-a show that in the case of resolving boundary layer (cases 20 and 5), no difference is made using periodic boundary; while with y^+ =6.4 (cases 21 and 8) a slight difference is seen behind the hub (Fig. 4-b).

In a steady state simulation, rotating-stationary interaction is approximated by a frame change modeling such as frozen rotor or stage (it will be discussed in detail later in 4.1.3). But in a transient simulation, the real rotating-stationary interaction can be captured.

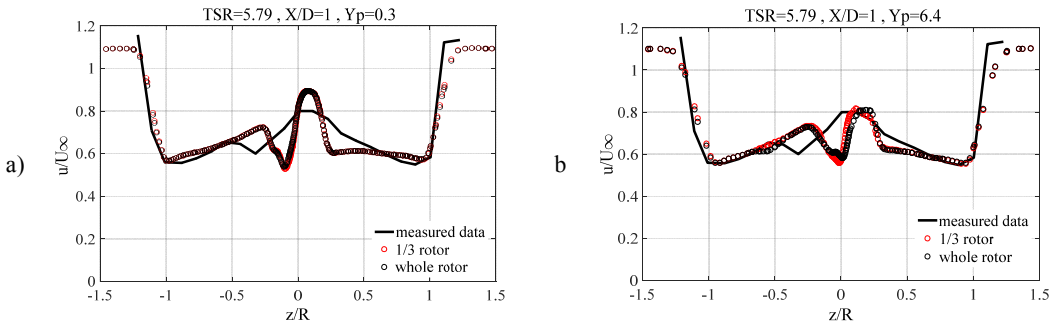

Fig. 4. Comparison of wake profile modeling 1/3 of the rotor and the whole rotor in design speed at X/D=1 with a)y^+= 0.3 (case 19) b) y^+= 6.4 (case 20).

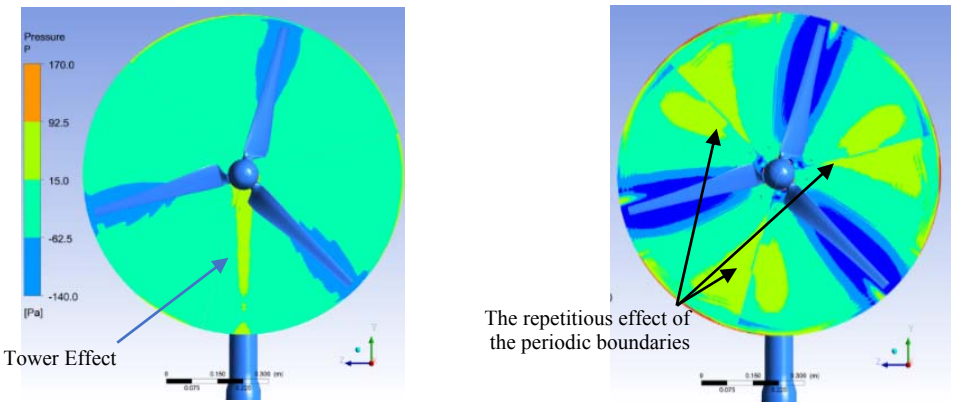

Fig. 5. Pressure variation from the transient results; left: full rotor modeling (case 14 of table2), right: periodic boundaries.

To take into account the effect of the tower, transient simulations considering the whole rotor are necessary. The flow near the blade is influenced when passing near the tower, and so the flow condition is different from the other two blades on top of the rotor. Thus, each blade has a specific boundary condition and therefore only one-third of the rotor cannot be used as the representative model of the whole rotor.

With the assumptions of periodicity on both sides of one rotor sector (1/3 rotor), the effect of the tower is missing in a transient simulation. Figure 5 shows two pressure contour plots from two transient simulations including the whole rotor (left) and 1/3 of it (right) in the same position of the blades. No effect of the tower is seen in the case of periodic boundaries as the three sectors are supposed to be the same. By modeling the whole rotor instead, the tower effect is seen in the pressure contours which influences downstream of the rotor as well (not shown here).

Near wall treatment

As explained in 3.2, the main difference of k- ω SST and k-ε turbulence models comes from the formulation in the boundary layer and the wall treatment modeling. To evaluate the effect of the modeling differences on the load calculations, cases 5 and 8 from Table 2 are considered. Steady state simulations are performed at the design operating point of the wind turbine using k- ω SST and k-ε (cases 22 and 21).

The cases 8 and 21 use the mesh with an average y^+ of 58. Then, the wall functions are used in both wall treatments as y^+ is above 11. Therefore, the main difference is between the ω and ε formulation inside the boundary layer. The thrust and power coefficients change by 3% and 15%, respectively. Furthermore, the use of the k-ε turbulence model leads to a periodic fluctuating result with an amplitude of 5-6%, which decreases the accuracy.

In cases 5 and 22, the same type of simulation is performed using a mesh with an average y^+ of '6.4'. Since the y^+ is below 11, two wall functions performances are totally different for two turbulence models. The results of two turbulence models show 1.9% and 3% differences in thrust and power coefficients, respectively; while the difference between the drag of the entire machine (including the tower and the nacelle) is around 10%. Since the load coefficients are integral values, they are not indicators of the flow details because the errors may compensate each other over the domain considered to give a correct value. A noticeable difference between k-ε and k-ω SST is expected using a mesh with an average y^+ below 11, as CFX 'scalable wall functions' used with the k-ε simplifies the flow variations in some parts of the boundary layer; while the k- ω SST takes into account the whole sublayer through its mixing formula with automatic wall function. Figure 6-a confirms this explanation, though at the downstream wake (X/D=4), the gap between two models becomes clearer.

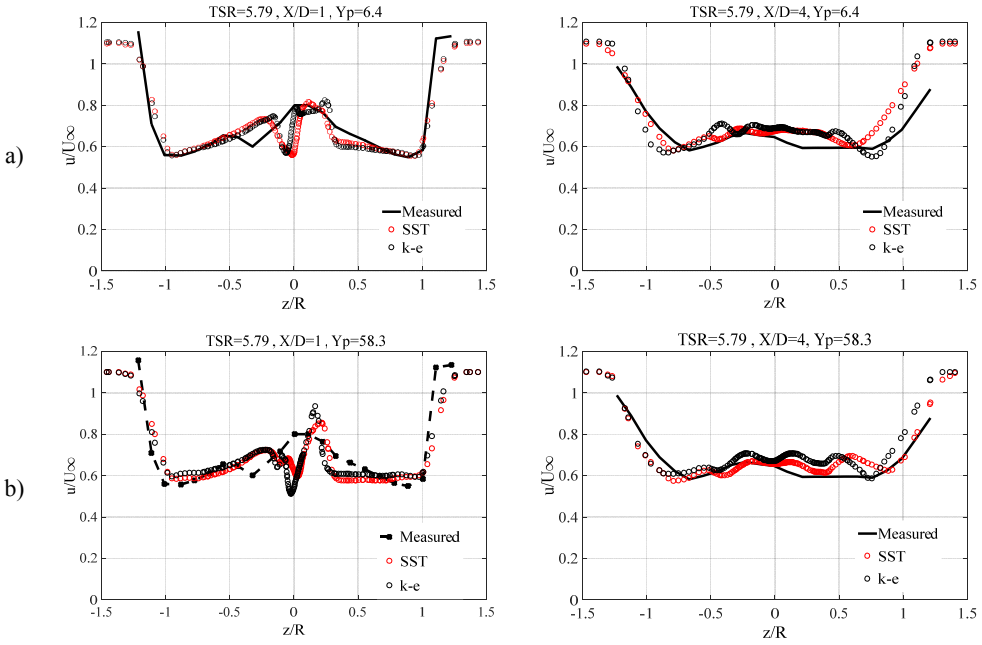

Fig. 6. Comparison of wake profile in the cases of different turbulence modeling in design speed with a)y^+=6.4 (case 5, 22 of Table 2) b) y^+=58.3(case8, 21 of Table 2).

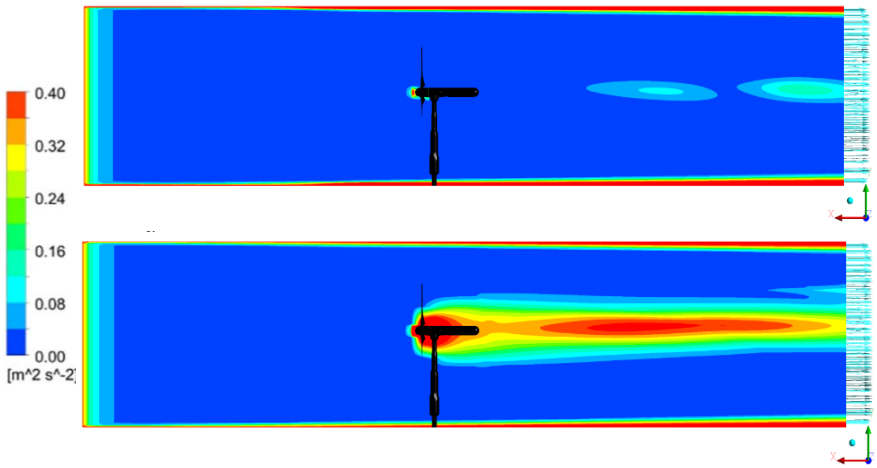

Fig. 7. Turbulence Kinetic Energy contour on a longitudinal plane for top: k-ε (Table 2, case 22); bottom: k- ω SST (Table 2, case 5).

In Fig. 6-b in which y^+ is above 11, both turbulence models are using wall functions. Although using the ω equation results in better matching with experiments, the difference with the k-ε model is not significant. The difference is more distinct farther downstream, which mainly comes from the different formula for the energy diffusion used in two models (Peng, Davidson, & Holmberg, 1996).

Figure 7 reveals more details in the difference between two turbulence models. Although they differ in the boundary layer region through eddy dissipation and eddy viscosity equations, they also differ in the turbulent kinetic energy since the two turbulence equations in each model are coupled together. As the effects are transmitted downstream, the gap between the velocity profiles is larger at X=4D, due to the different diffusion formula in the two models. In the center parts, in which the flow is affected by the presence of the nacelle body, different velocity profiles are obtained with different boundary layer calculations of the two models.

Rotating-Stationary Domain Interaction

For a steady simulation, it's needed to model the relative motion of the rotor towards the stationary components such as the tower. There are two options to model the frame changes in a steady state simulation, in which the flow motion is watched at a fixed time.

In 'stage' method (as named in CFX) a mixing plane mixes the flow at the interface of the

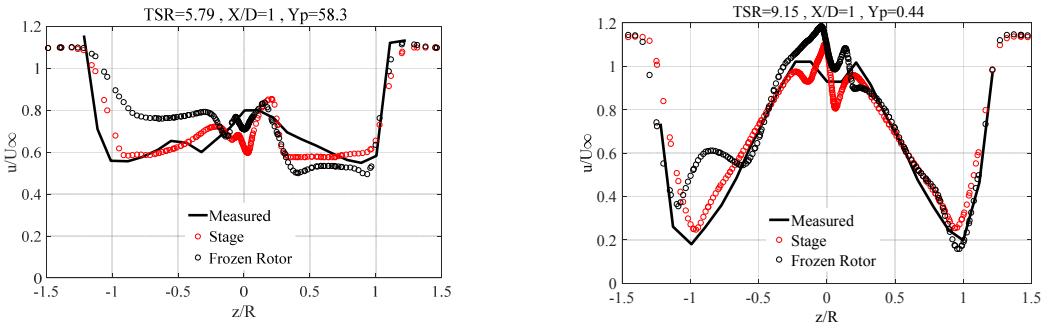

Fig. 8. Comparison of wake profile at X/D=1 in the cases of stage and frozen rotor interfaces in design and high speeds respectively with y^+=58.3 (left : cases 8 and 23 of table 2) and y^+=0.44 (right cases 3 and 24 of table 2).

stationary and rotating domains. The average values are applied on the interface for upstream and downstream components. While in the 'frozen rotor' method the two frames of reference connect in such a way that each stay in a fixed relative position throughout the calculation.

Although 'stage interface' is selected as the main approach of this paper, we have studied the sensitivity of the results to the frame change model. A study is performed applying frozen rotor interface at design operating point (Table 2, case 23). Using a coarse mesh with y^+=58, it shows 1% difference in thrust coefficient in compare to the similar simulation with stage interface (Table 2, case 8). The difference in power coefficient is around 8%.

In the case of resolving the boundary layer (Table 1, case III) and at an off-design point with TSR=9 (Table 2, case 24), the deviation from the similar 'stage' simulation (Table 2, case 3) in thrust coefficient is about 1 % whereas the power coefficient changes around 4 %.

Although the mentioned difference between the load coefficient values is not too much, looking at the wake profiles reveals the main differences. Figure 8 shows that especially in the case of using wall functions (y^+ =58), 'frozen rotor' interfaces lead to large differences. Resolving the boundary layer (y^+<1) decreases the difference (Fig. 8-right); while stage simulation is closer to the experimental data. The 'frozen rotor' model causes a major asymmetry in the flow field because it ignores the variations of the rotating blades positions towards the stationary domain. The frozen rotor modeling disregards the rotating flow variations towards the stationary parts (like the tower) during the rotation and assumes a uniform situation for each side of the rotor It can be concluded that although resolving the boundary layer decreases the dependency on the frame change model, the error due to the frozen rotor simplification cannot be ignored in the case of wall function being used.

Transient Simulation Convergence

In order to see the numerical aspects of different solving methods in a transient simulation, it is needed to look at their performance regarding the convergence process and the results.

During a transient simulation, the flow needs some time to develop. Regarding the rotation speed at the design point, roughly speaking, the time for the axial flow to reach the domain far downstream ($t=X/U\infty$) is equivalent to the time duration of six rotor revolutions ($6\times 2\pi/\Omega$). In other words, when the rotor has rotated 6 turns, the flow downstream of the rotor at X/D=4 starts to be affected by the rotation. Although the transient simulations are initiated from a steady state flow, it takes time for the flow to become stable, and this convergence time varies based on the grid (space discretization), rotational speed, turbulence modeling, etc. For integrated parameters (load coefficients), the convergence is met sooner than the velocity profiles in the wake. Furthermore, the velocity fluctuations amplitude is different in each case. The following statements are perceived out of the simulations. To be sensible, the simulation time is described in terms of the equivalent number of rotor complete rotation.

- In low tip speed ratio, convergence is reached faster than at high speeds. Even for the central regions of the wakes, it converges after 6 rotations.
- Using a refined mesh causes a faster convergence. For example, at TSR=6 the load coefficient solutions are converged after 15 rotations with y^+ of 58 compared with 10 rotations in the case of y^+=0.3.
- SAS-SST turbulence model leads to larger fluctuations which vanish slower than with the SST model.

In the central region behind the nacelle ($|z|<0.5$), the numerical convergence cannot be reached easily. There are inherently intensive fluctuations in flow pressure and velocity during the simulation time. Even in the final result, these semi-periodic fluctuations don't disappear completely. So there are more uncertainties in these regions which vary from 2 to 5%.

Time Step Sensitivity

In order to check the independence of the results

from the time step size, a sensitivity analysis was performed. It should be a compromised between the computational expenses and the solution accuracy.

The number of time steps per rotation is chosen to be 120, i.e., a rotation path of three degrees in each step of the solution is considered. It equals to 2.5×10-4 seconds regarding the angular velocity of the rotor. Time step sensitivity analysis showed that it is the maximum time step size allowing an acceptable solution. If the time step size reduces to one-third, i.e., 360 time-steps per rotation period, the difference in the results is below 1.6% in maximum.

4.2 Performance Characteristics

Thrust coefficient CT and power coefficient CP are engineering quantities representatives of the machine performance. They are presented at different TSR. Three different meshes have been used to perform the simulations (Table **2**) and the results are compared.

The same formula as in the experiments is used to calculate the load coefficients. The reported experimental data for CT have, however, been calculated based on a vague method of drag (D) evaluation on the stationary part, i.e., hub, nacelle, and tower, which decreases the accuracy of the validation (described in Section. "Test Case") It is seen also in the simulations that the various modeling methods work very differently in the evaluation of thrust on the stationary parts.

Figures 9 and 10 show the measured power and thrust coefficients as a function of TSR for the cases 1-18 of Table **2**. Included in the graphs are three different grids (cases I-III of Table 1). For the transient simulations, the load variations are calculated during the simulation time. Although there are some inherent fluctuations in a transient rotation process, it takes time for the numerically induced fluctuations to be damped and the solution converges, (see "Transient Simulation Convergence"). The time averaged values are calculated over one period.

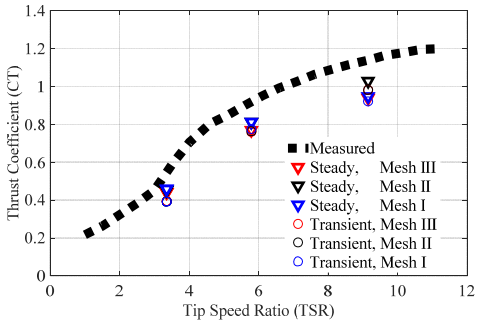

Fig. 9. Comparison of thrust coefficient from CFD with the measurements.

In general, the agreement between the measurements and CFD is better for the power coefficient than thrust coefficient. Calculated CT from the simulations is 0.09-0.11 below the experimental data for different TSR. The measured C_p values are almost captured by CFD at both design and high rotational speed, while it deviated by 0.05 from the measured value at a low TSR. Since the values of load coefficients are close to zero, the errors are reported as the deviation, i.e. the difference between the calculated and the simulated values.

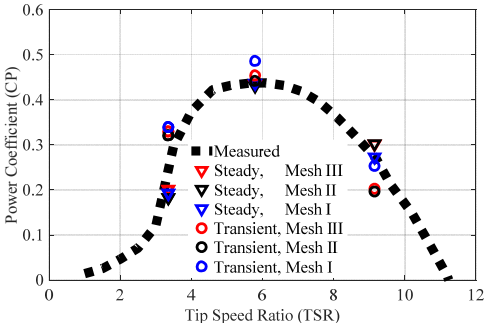

Fig. 10. Comparison of power coefficient from CFD with the measurements.

Power coefficient is mainly related to the torque acting on the turbine. Thrust coefficient is mainly related to the drag and thus the wake behind the turbine, in which more sources of energy loss may make changes. Furthermore, the experimental method used to evaluate the drag on the stationary parts is an issue which provides a special experimental data for C_T.

The transient results are not necessarily closer to the experiments for the thrust and power coefficients. But, it is seen later in this paper that a transient simulation improves the wake results significantly. Load coefficients are integrated value of a load distribution on the blade, nacelle, and tower. Such parameter does not guarantee the correct distribution even though the integrated simulated values match better with an experimental one. Detailed analysis of the wake profiles will allow gaining further information.

Looking at both the steady state and transient simulations, the results of Mesh II and Mesh III are similar, while using the latter one imposes 90% extra density on the mesh (Table 1). When the automatic wall functions (k-ω SST model at $y^+<11$) are used for the integrated parameters, further resolving the boundary layer produces no better results, i.e. the mesh with $0<y^+<11$ work similarly. Indeed, the automatic wall functions can provide a reliable wall treatment when the mesh is fairly refined in the cases 4-6 and 13-15 (Table **2**) in which the average y^+ is around 6 (in design speed). In this case (Table 1: case II), the grid size reduces by 90% compare to the case of the fully resolved boundary layer (Table 1:case III).

4.3 Wake of the Model Wind Turbine

The wake of a turbine is characterized by a velocity defect, high turbulence level, and helical tip vortices (Krogstad & Adaramola, 2012). The rotational speed (or TSR) determines the level of interaction

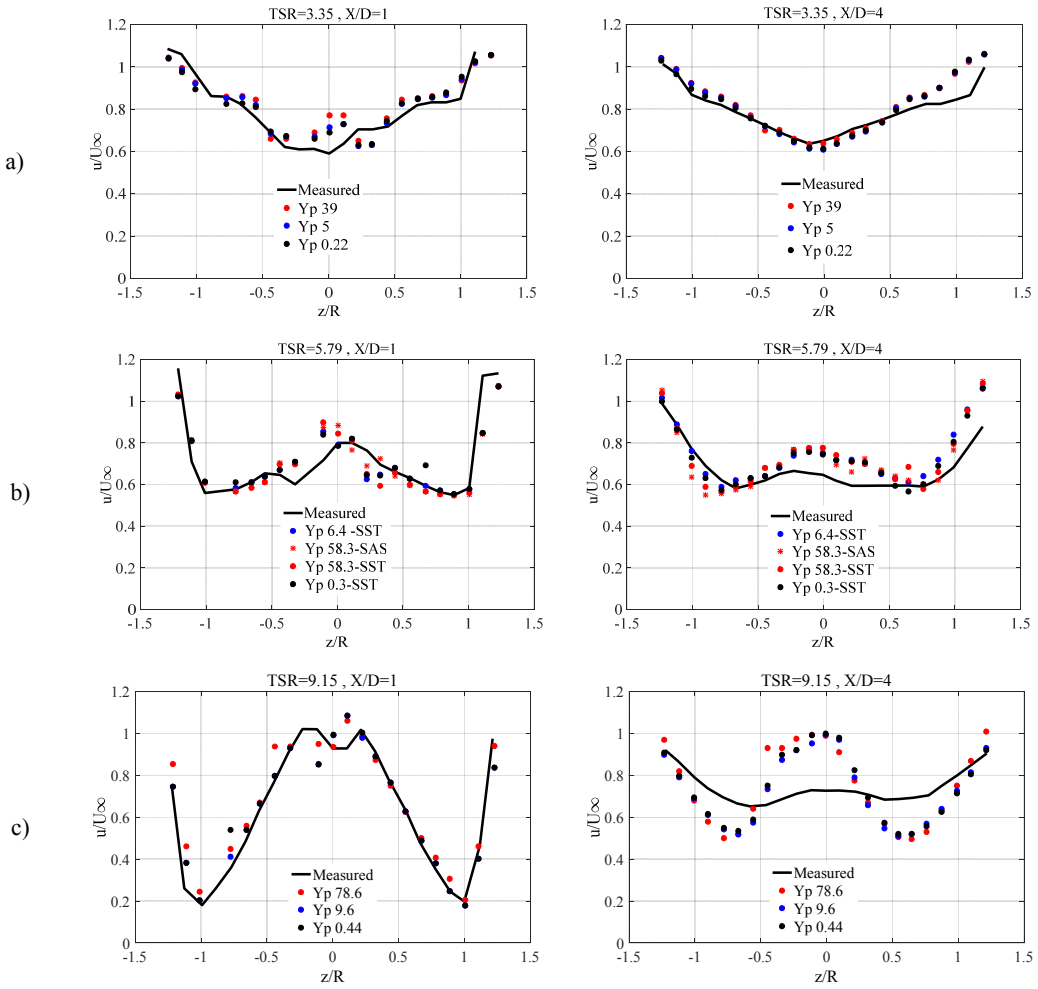

Fig. 11. Time-averaged profile of axial velocity at the hub height for four positions downstream of the rotor plane with three different mesh resolutions for a) TSR=3.35 (cases 1,4,7), b) TSR=5.79 (cases 2,5,8), c) TSR=9.15(cases 3,6,9).

between the air flow and the rotor, and hence determines the characteristics of the wake velocity deficit. Irrespective of the TSR, the wake velocity depends on the radial position in the transversal plane. The wake region gradually widens as TSR increases, in agreement with the increase in CT (Fig. 9) (Krogstad & Adaramola, 2012).

The wake axial velocity distribution can be classified into three regimes: the stalled operation or low TSR regime, the optimum TSR regime, and the propeller performance or high TSR regime. This classification is directly related to the performance characteristics of the model turbine (Krogstad & Adaramola, 2012).

A summary of the effect of the TSR on the axial velocity profile in the near wake (X/D=1) of the model turbine is presented in the profiles measured in (Krogstad & Adaramola, 2012) at the hub-height transversal lines. Wake velocity field development was also investigated through the velocity profile at X/D=4. In the transient simulations (Table 2, cases 10-18, 25), for each of the points on the lateral lines, there is a time-varying velocity. Considering a time averaged value for each point results in the plots of Fig. 11.

The simulation results for the axial velocity profile at hub height were analyzed for nine steady state simulations (Table 2: cases 1-9) with three different mesh resolutions and y^+ values (Table 1: cases I-III). Details can be found at Table 1.These results are plotted only for high TSR in Fig. 12 besides the corresponding wind tunnel experiments. In the legends of Figs. 11 and 12, only the y^+ values are mentioned.

Near wake of the Model Turbine

For the low TSR where the velocity defect is most significant in the blade root region, the wake velocity distribution (Fig. 11-a) resembles the deficit field found behind a circular bluff body. The streamwise velocity deficit is highest in the vicinity of the hub and then reduces gradually outwards. Velocity deficit is not too much near the rotor tip as the generated torque has been low. Because of the low-velocity defect in the near wake of the turbine at low tip speed ratios, this regime is characterized by low thrust and power coefficients (see Figs. 9 and 10).

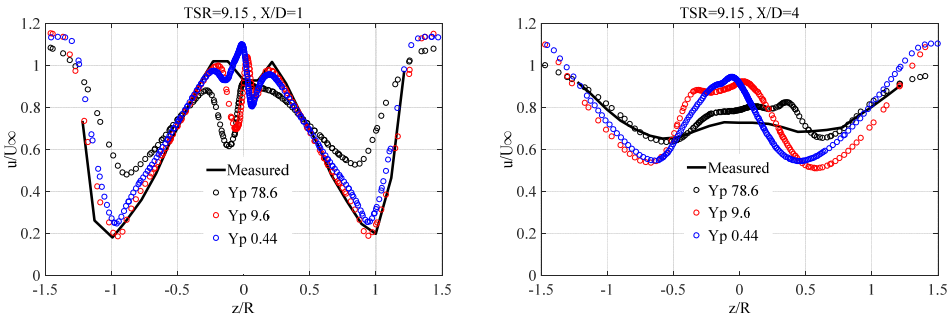

Fig. 12. Steady state profile of axial velocity at the hub height for four positions downstream of the rotor plane with three different mesh resolution for TSR=9.15(cases 3,6,9).

The level of the velocity deficit behind the hub is a challenge for the numerical simulation methods in this case. The outward velocity increment is modeled properly by simple meshes and even skipping the transient effect but to model the central part of the profile, transient effects are necessary to be considered. Fully resolving the boundary layer in transient simulations helps to catch the corresponding velocity deficit behind the hub.

In the case of the optimum TSR regime, the velocity defect is stronger than for the low TSR regime and is relatively constant within the rotor diameter region (-R<z<R) with a small reduction in the hub region (Fig. 11-b). This shows that the rotor operates very efficiently at this condition. Thus, more energy is extracted from the air flow and the energy is extracted uniformly across the rotor plane as the velocity deficit is more uniform throughout the rotor diameter (-R<z<R).

At the design point, a transient simulation and fully resolving the boundary layer (y^+<1) are required to catch the velocity deficit behind the hub. For the rest (>0.5R), transient effect doesn't influence the profiles. For estimating of the outer parts of the velocity profile (>0.5R), only a coarse mesh and wall functions are enough with a steady state simulation (not shown here for this TSR). Also, the wake velocity profile calculated based on SAS-SST model (Table 2, case 25) is plotted as well as the SST model (Fig. 11-b). No improvement in the calculated loads are observed compare to the SST model while imposing more fluctuations in the time history of the results. It can be concluded that resolving the boundary layer is more effective to capture the velocity deficit in the near wake, comparing to the turbulence modeling.

The strong radial variations in the velocity deficit are seen at the high TSR regime (Fig. 11-c). At the center of the flow (Z 0) the velocity seems not to be affected by the rotation and u ≈ U∞. It may be due to the wake spreading direction which will be discussed later in this paper. The transient simulations have captured the velocity profile properly irrespective of the mesh resolution. In this operating mode, the inner part operates as a propeller providing additional energy into the central part of the wake, which may be observed as a very small velocity defect (10% of U∞) downstream of the hub (-0.1R<z<0.2R based on the measured data). The outer part of the blade (near the blade tip) operates at a low angle of attack, and so it is only the midsection of the blade that actually operates in an efficient turbine mode. Hence, this is where the strongest velocity defect is found in the wake (Fig. 11-c). The flow velocity defect, in this case, is much more than the design speed, as the velocity decreases to 20% of U∞ near the rotor tip. The flow in the wake at this operating condition is therefore characterized by strong velocity gradients, and the corresponding high shear generates high turbulence levels in the wake (Krogstad & Adaramola, 2012). For the high TSR regime, the power coefficient is low, whereas the thrust coefficient is very high (Figs. 9 and 10) as the airfoil lift force is rotated towards the streamwise direction (Krogstad & Adaramola, 2012).

As seen in a steady state simulation (Fig. 12), the velocity deficit near the rotor tip cannot be modeled with a coarse mesh and wall functions. Mesh refinement and resolving the boundary layer provide a proper numerical model at this part even if the time variation is skipped. When it comes to the central part of the velocity profiles, it is only the transient simulation that can catch the sudden velocity increase behind the hub. Considering the time variations in a transient simulation, it is not required to resolve the boundary layer. A coarse space discretization can be sufficient to get the near wake profile in this case.

The time-averaged measured streamwise (axial) velocity contour plots in the upper section of the turbine wake at X=1D downstream of the model turbine are presented in Fig. 13 for TSR=9.15, as well as the steady state simulation results. The velocity is normalized by the freestream velocity, and the length is normalized by the rotor radius. At a high TSR, a large radial inhomogeneity in the velocity defect is raised (Fig. 13). In agreement with hub height velocity profiles (Fig. 11-c), there is a slight velocity deficit near the wake center and a strong velocity reduction near the rotor tip. Although a steady state result is plotted, the contour matches properly with the one from the measurements and the main trend is captured.

Furthermore, the variations are radial, as expected. So, the velocity profile on the hub height line was

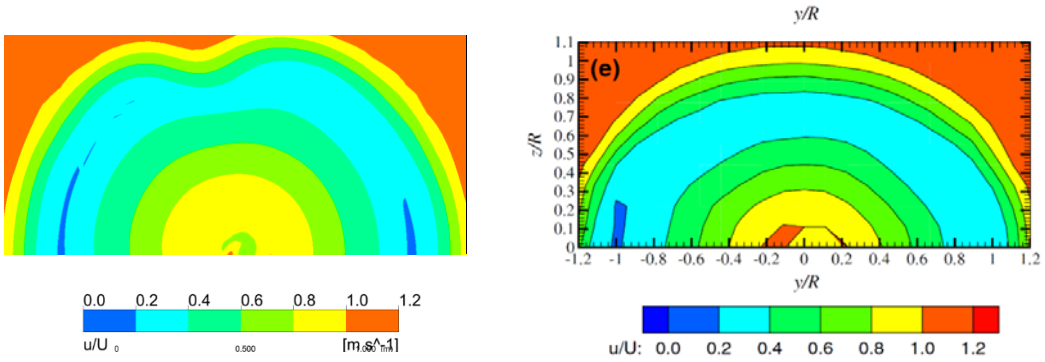

Fig. 13. Contour plots pf streamwise velocity component in the wake at X/D=1 for TSR=9.15. Left: steady state simulation (case5 of Table 1) right: time-averaged measured data.

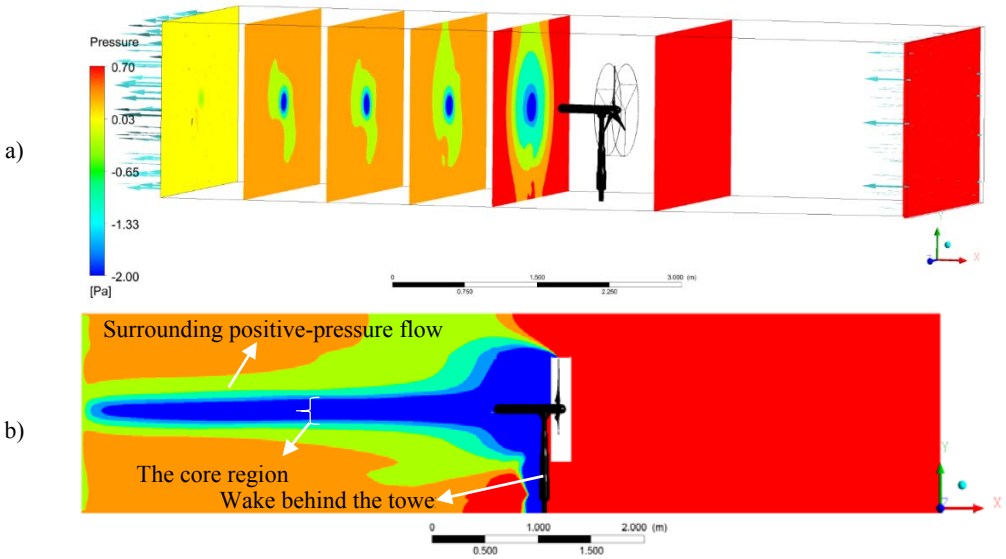

Fig. 14. Contour plots of the pressure at different cross-sections and at the mid plane. (case 5, Table 2).

taken as the representative of the wake profile.

Wake Velocity field Development

Figure 14 shows contour plots of the pressure on certain planes from the inlet to the outlet of the wind tunnel. For the design operating point (TSR6), different planes at four axial distances (1,2,3 and 4 times of the rotor diameter) downstream the rotor are shown as well as a plane upstream. There is no significant variation from the inlet plane upstream to the rotating domain (Fig. 14-a), though the upstream just before the rotating part is influenced by the rotation slightly (not shown here due to the specified range of variations in the plot).

The static pressure drops gradually downstream of the rotor as the flow is passing through the tunnel towards the outlet. A radial distribution is raised in each transversal plane due to the radial energy diffusion at the swirling wake (Fig. 14-a). The pressure at the central part of the rotation is less than the ambient pressure. The pressure increases radially from the center of the wake to reach the pressure of the free stream.

The entrainment of the momentum from the surrounding freestream into the wake makes the low pressure in the wake recovers faster. At the near wake, the region surrounding the core is still at the same pressure as the rotor upstream. As the downstream distance increases, the mixing leads to a pressure decrease in these surrounding regions, while the low-pressure core part is becoming smaller. As seen in the wake profiles in Fig. 11-b, the width of the wake core decreases around 40% when it is 4D downstream of the rotor. Wake core is the central tube, in which the pressure gradient is high. On the other hand, irrespective of the TSR, the whole wake width increases with the downstream distance due to the flow mixing (Krogstad & Adaramola, 2012). Inside the wake region, the velocity is low in addition to the low static pressure. This leads to a low energy region inside the wake that will be discussed later in this paper. Figure 14-b shows how the pressure in the wake varies in the vertical central plane (XY plane at z=0) at the design point. The low-pressure region orients from the rotor tip. This core region is surrounded radially by high positive pressure. Furthermore, behind the tower is covered by a

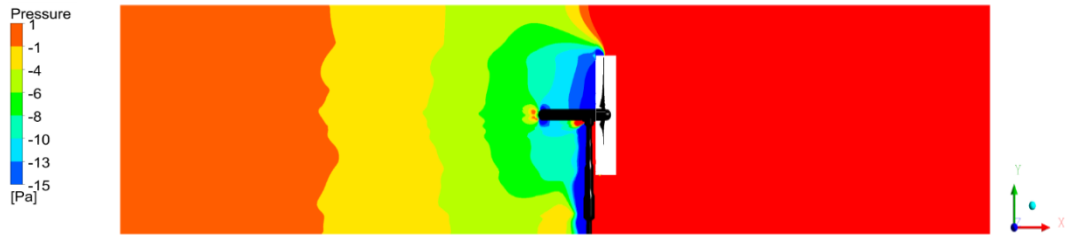

Fig. 15. Pressure profile at the central axial plane for high TSR (case 6,Table 2).

wake. At a lower TSR (not shown here), the low-pressure region is more limited and completely enclosed by the high-pressure non-swirling flow out of the wake.

For a high rotational speed (TSR=9), the pressure development is presented in Fig. 15 at a vertical central plane. The flow leaving the rotor tip has a large vertical component. It causes the tip vortices to move toward the top wall of the tunnel. In this case, the low-pressure flow region is not surrounded by a high-pressure flow, but the whole area is filled with a low-pressure flow. An adverse static pressure gradient occurs downstream of the rotor. It was observed (not shown here) that at each axial streamline inside the wake region, the total pressure is increasing as well as the both velocity and the static pressure. Increasing the total pressure is the effect of momentum entrainment from the freestream into the wake. Consequently, the surrounding region becomes narrower and the wake widens as the streamlines are moving outward. At the surrounding streamlines, there is no significant change in the total pressure. So, the velocity decreases when the static pressure increases. Overall, the dominant phenomenon the downstream the rotor is mixing of the wake with the freestream. The velocity deficit at the near wake recovers further downstream and the flow becomes more uniform.

Looking back at Fig. 11, the streamwise development of the wake can be further investigated. At a low TSR, the velocity profile is more uniform at X/D=4 compare to the near wake at X/D=1 (Fig. 11-a). The width of the low-velocity core region is smaller. The simulation results show that a coarse mesh is enough to model this case if the transient effects are considered.

Near the design tip speed ratio (Fig. 11-b), the steep initial gradient decreases quickly with the streamwise distance because of the moment entrainment from the freestream into the wake. As the downstream distance increases, there is a gradual increase in the wake width and a corresponding reduction in the velocity defect as the flow gradually develops towards a conventional wake. The wake behind the nacelle is clearly visible at the first station but is smeared out quickly further downstream. The core region at the center of the profiles is smaller at X/D=4. At the near wake, the core region was one diameter wide, which decreases to around 70% far downstream. This decrease is the result of the flow mixing. The dense meshes performed better in this case, while the SAS SST turbulence model with a coarse mesh has been less accurate.

The dependency on the streamwise distance is more pronounced for the higher tip speed ratios (Fig. 11-c). Initially at X/D=1, there was a very high streamwise velocity near the wake center and a strong velocity reduction near the rotor tip. As the downstream distance increases, this strong non-uniformity is quickly reduced. This is partly due to the mixing caused by the tip vortices and partly caused by turbulent diffusion in the strong shear layers. Similarly, the high velocity near the center is gradually reduced because of the radial energy diffusion (Krogstad & Adaramola, 2012).

Considering the transient effects in the simulations, all the three mesh resolutions work similarly to model the wake development. When the mesh is fine enough in the steady state simulation (Fig. 12), the velocity is recovered from the near wake to the far wake. It shows that the flow mixing can be modeled in spite of skipping the transient effects.

Overall about the steady state simulations, the main shortage to model the near wake was behind the hub, while these types of simulations calculated the rotor tip velocity deficit properly. Far downstream when the flow is more uniform and there is less pressure gradient, the steady state results can be as reliable as the transient simulation results and the radial energy diffusion can properly be estimated. But, if the mesh is too coarse as the case I (Table 1), then the results of the steady state simulation is incorrect. In Figure 12, although the velocity profile of the coarse mesh (high y^+) seems to be closer to the measured values, it is not reliable. Because considering the same simulation results at X/D=1, basically the velocity deficit is not captured at X/D=1. So, the velocity recovery is around 14% while it should be around 55%.

Generally, in the wake development behind the rotor, the turbulent and energy diffusions play the main role, since the dominant phenomenon is the dissipation of the wake while mixing with the free stream. Therefore, the low accuracy of the simulation results downstream at high TSR shows the limitation of the model used in this condition. The turbulence model k-ω SST includes the addition of a cross-diffusion term in the ω equation and a blending function to ensure that the model equations behave appropriately in far-field zones (Peng *et al*., 1996), but it is still not accurate enough to recover the velocity deficit at the propeller regime of the wind turbine performance.

5 CONCLUSIONS

Looking for a methodology to estimate the loads acting on the blades, the performance of a model turbine, as well as the wakes formed by the rotor, has been calculated through a numerical study. A multiple frame of reference approach is considered to simulate the rotating domain around the blade and the stationary flow inside the wind tunnel in which tower and nacelle are also included. To evaluate the adequacy of wall functions to model the near-wall flow, different meshes have been created in both rotating and stationary domain based on the multi-blocking structured hexa mesh of ICEM. Applying shear stress transport model makes it possible to use automatic wall functions which are investigated with different y+ values. RANS equations have been solved by ANSYS CFX solver. Computational domain consists of 52 million nodes to resolve boundary layer. Time-averaged values of the performance parameters as well as the wake velocity profiles have been calculated out of the transient simulations. The power generation and the thrust force are calculated through different methods assuming steady and transient simulation, as well as the velocity profiles in the wake downstream of the rotor. Both near wake and the wake development are studied. Key findings based on current study are discussed below:

1. In general, the agreement between the measurements and CFD is better for the power coefficient than thrust coefficient. For the estimation of the integrated parameters, the transient results are not necessarily closer to the experiments in neither of the thrust and power coefficients, while a transient simulation improves the wake results significantly.
2. The near wake profiles resulted from the transient simulation match well with the experiments at all the TSR range. A coarse or fine mesh influences slightly the transient numerical results. For the wake development modelling at high TSR, the present simulation needs to be improved, while at low and moderate TSR the results match with the experiments at far wake too.
3. At the near wake velocity profile, the more velocity defect and the more uniformity at its radial distribution (across $-R<z<R$) are two indicators of a more effective performance of the rotor. From these two, the velocity deficit at the rotor tip is easy to model, but the radial distribution estimation is challenging for a numerical model.
4. The main shortage of the steady state simulation to model the near wake was behind the hub, while these types of simulations calculated the rotor tip velocity deficit properly.
5. The difference between the k-□ and k-ω SST turbulence models, relates to both the wall treatment and the flow diffusion, i.e. the wake development. At lower y+ the difference is more distinct.
6. Fully resolving the boundary layer in transient simulations helps to catch the velocity deficit profile behind the hub while the outward velocity increment is modeled properly by simple meshes and even skipping the transient effect. Transient effects are necessary to be considered to model the central part of the velocity profile. Transient simulations deliver results in a close agreement with the experimental wake profiles.
7. In a steady state simulation, the periodicity is a proper assumption if the mesh is refined enough and the boundary layer is fully resolved. Otherwise, the accuracy decreases especially in the thrust evaluation of the whole machine. Only in a transient simulation, the real rotating-stationary interaction can be captured. The periodicity assumption doesn't work in this case, since the effect of the tower is missing with the assumptions of periodicity on both sides of one rotor sector (1/3 rotor).
8. Considering the transient effects in the simulations, all the three mesh resolutions work similarly to model the wake development. At the both steady state and transient evaluations of the integrated parameters, when the automatic wall functions (k-ω SST model at $y+<11$) are in used, more resolving the boundary layer has no advantages, i.e. the mesh with $0<y+<11$ work similarly.
9. Resolving the boundary layer helps reach convergence faster; while it increases highly the number of nodes in the mesh. Furthermore, the amplitude of the fluctuations in the results is lower than with wall functions (coarser mesh). Although a periodic oscillating result is expected from an unsteady rotation phenomenon, refining the mesh helps to remove the high oscillations coming from the numerical uncertainties in the zones with high-pressure gradients.
10. Since the velocity recovery from X/D=1 to X/D=4 is captured in the steady state simlulations, it shows that this type of simulations can model the downstream flow mixing, but only in the case that the mesh is fine enough to resolve the boundary layer.
11. At the propeller regime of the wind turbine performance (high TSR), the turbulence model of k-ω SST is not still accurate enough to model the dissipation of the wake while mixing with the free stream, and velocity deficit is not recovered completely. It is suggested not to use the eddy viscosity hypothesis in this case, and apply the Reynolds stress turbulence models or LES in the next step.
12. The flow radial diffusion is more complicated in the case of high TSR, as the swirling flow in the wake behind is under a high-pressure gradient.

REFERENCES

Adaramola, M. S. and P. Krogstad (2011). Experimental investigation of wake effects on

wind turbine performance. *Renewable Energy* 36(8), 2078-2086.

ANSYS (2009). *CFX-solver manager user,s guid.*

ANSYS (2013). *CFX-solver modeling Guide Release 15.0*

ANSYS (2013). *CFX-solver theory Guide Release 15.0*

Bechmann, A., N. N. Sørensen and F. Zahle (2011). CFD simulations of the MEXICO rotor. *Wind Energy* 14(5), 677-689.

Carrión, M., R. Steijl, M. Woodgate, G. Barakos, X. Munduate and S. Gomez-Iradi (2015). Computational fluid dynamics analysis of the wake behind the MEXICO rotor in axial flow conditions. *Wind Energy* 18(6), 1023-1045.

CFD online (2011). https://www.cfd-online.com/Wiki/SST_k-omega_model.

Frohboese, P. and A. Andreas (2007). Effects of icing on wind turbine fatigue loads *Journal of Physics: Conference Series* 75.

Gomez-Iradi, S. and G. N. Barakos (2008). Computationalfluid dynamics investigation of some wind turbine rotor design parameters. *IMechE* 222, 455-470.

Gomez-Iradi, S., R. Steijl and G. N. Barakos (2009). Development and validation of a CFD technique for the aerodynamic analysis of HAWT. *Journal of Solar Energy Engineering* 131.

Hansen, T. (2010).*Wind turbine simulations using navier-stokes CFD.* Master's thesis, Royal Institute of Technology; CMR Prototech, Sweden

Homola, M., M. Vrik, P. Nickelasson and P. Sundsbo (2011).Modelling of ice induced power losses and comparison with observations *Winterwind conference,* Sweden

Kalvig, S. and E. Manger (2011). Wind turbine simulations comparing the actuator disk approach with a fully resolved rotor simulation, *7th EAWE PhD Seminar on Wind Energy in Europe,* Delft, Netherlands, 67-70. Delft University of Technolog.

Kalvig, S., E. Manger and B. Hjertager (2014). Comparing different CFD wind turbine modelling approaches with wind tunnel measurements. *Journal of Physics: Conference Series* 555.

Karlsen, J. A. (2009). *Performance calculation for a model turbine.* Master thesis in Energy and the Environment, Norwegian University of Science and Technology, Norway.

Krogstad, P. and J. A. Lund (2012). An experimental and numerical study of the performance of a model turbine. *Wind Energy* 15(3), 443-457.

Krogstad, P. and M. Adaramola (2012). Performance and near wake measurements of a model horizontal axis wind turbine. *Wind Energy* 15, 743-756.

Krogstad, P. and P. E. Eriksen (2013). "Blind test" calculations of the performance and wake development for a model wind turbine. *Renewable Energy* 50, 325-333.

Krogstad, P., J. A. Karlsen and M. Adaramola (2010). Performance of a model wind turbine, *17th Australasian Fluid Mechanics Conference*, Auckland, New Zealand.

Lutz, T. (2011). Near wake studies of the MEXICO rotor, *EWEA Annual Event,* Brusseles.

Menter, R. (2012). *Best practice: Scale-resolving simulations in ANSYS CFD*, ANSYS Germany GmbH

Oggiano, L. (2014). CFD simulations on the NTNU wind turbine rotor and comparison with experiments. *Energy Procedia* 58, 111-116.

Peng, S., L. Davidson and S. Holmberg (1996). *The two-equation turbulence k-ω model applied to recirculating ventilation flows*. Chalmer University of technology, Göteborg, Sweden.

Reid, T., G. Baruzzi, I. Ozcer, D. Switchenko and W. Habashi (2013). FENSAP-ICE simulation of icing on wind turbine blades, part 1: Performance degradation, *51st AIAA Aerospace Sciences Meeting including the New Horizons Forum and Aerospace,* Texas.

Schepers, J. G. and R. Van Rooij (2008). *Analysis of aerodynamic measurements on a model wind turbine placed in the NASA-ames tunnel*, ECN's and TUD's contribution to IEA Wind Task XX.

Schepers, J. G., K. Boorsma, T. Cho and S. Gomez-Iradi (2012). *Analysis of mexico wind tunnel measurements*, Energy Research Centre of the Netherlands (ECN).

Schreck S. (2008).*IEA wind annex XX:HAWT aerodynamics and models from wind tunnel measurements*, National Renewable Energy Laboratory, Colorado.

Sørensen, N. N., A. Bechmann, P. Réthoré and F. Zahle (2014). Near wake reynolds-averaged Navier–Stokes predictions of the wake behind the MEXICO rotor in axial and yawed flow conditions. *Wind Energy* 17(1), 75-86.

Tammelin, B., M. Cavaliere, H. Holttinen, C. Morgan, H. Seifert and K. Säntti (1998). *Wind energy production in cold climate (weco)*, Finnish Meteorological Institute.

Turkia, V., S. Huttunen and T. Wallenius (2013). *Method for estimating wind turbine production losses due to icing,* VTT Technical Research Centre of Finland.

Van Rooij, R. and E. A. Arens (2008). *Analysis of the experimental and computational flow characteristics with respect to the augmented*

lift phenomenon caused by blade rotation, Delf University Wind Energy Research Institute.

Zhao, M., D. Jiang and S. Li (2009).Research on fault mechanism of icing of wind turbine blades, *World Non-Grid-Connected Wind Power and Energy Conference. IEEE*, Nanjing